PHYSICS LIMITATIONS ON CALORIMETRY

(Summary of a Contribution presented to the FNAL Workshop
on Calorimeters, May 9/10, 1975)

C.W. Fabjan and W.J. Willis
CERN, Geneva, Switzerland

In Table 1 we list the effects which are known to affect the energy resolution of calorimeters. Although most comments are generally valid, we will concentrate on ionization-measuring detectors (homogeneous and sampling type).

Side- and back-leakage of energy as a function of absorber size is shown in Fig. 1 1,2). The shower length increases logarithmically with energy; near-total containment of the shower is necessary for optimal energy resolution and suppression of low-energy tails in the response.

Sampling fluctuations are present whenever the ionization is not measured throughout the total volume but only at discrete points in the absorber. The effect on the resolution can be judged by Fig. 2, which shows the results of direct measurements of the sampling fluctuations 2); it is technically possible to achieve a fine-grained sampling, which does not limit the resolution 2,3).

Saturation in the response of the ionization-measuring medium for heavily ionizing particles is well known in organic scintillators 4). Such an effect on the energy resolution could be simulated with the CERN Fe/L Ar calorimeter 2) by lowering the high voltage to a value where recombination effects limited the measured energy. However, in the 4-10 GeV energy range no influence on the resolution was found.

Noise is always present in various forms such as photon statistics and amplifier noise, but the most serious instrumental effect may well be a non-uniform sensitivity to the ionization throughout the absorber, or limits in the obtainable calibration accuracy, or pile-up effects due to high particle rates.

Next we discuss the effects on the resolution due to the nuclear interaction.

Table 2 lists the Albedo for various particles and energies. The measurements are consistent with the Monte Carlo estimates showing this energy loss to become less important with increasing energy.

The energy loss due to escaping muons and neutrinos is estimated in Table 3 [6]. Again, this effect is small at low energies and decreases with increasing energy.

The mechanisms, which determine the energy resolution, are all associated with the nuclear interaction between the incident particle and the target nuclei and are often globally summarized as "binding energy" (BE) losses. The nuclear interaction is usually considered to proceed in three stages: within 10^{-22} sec of the passage of the primary particle, fast secondary particles are ejected ("cascade particles"). The multiplicity of this component shows

i) an extremely weak dependence on the mass A of the nuclei (factor of 1.8 between H and U) [7], at variance with predictions of the "Intranuclear Cascade Model";

ii) insensitivity to the type of the incident particle and to its energy in the range 30-500 GeV [7,8].

The remainder of the highly excited nucleus will de-excite within 10^{-18} to 10^{-13} sec with the emission of slow p's, γ's, and predominantly n's. In Fig. 3 some data and MC estimates are shown for energies up to ~ 1 GeV. The loss in visible energy due to the binding energy of the "evaporated" n's and p's is summarized in Table 4.

There are two direct consequences of this BE loss: the average visible energy produced by an electron (or π^0), for which these nuclear interactions are absent, will be greater compared to a hadron-initiated cascade (see also Fig. 4); consequently, the fluctuations in the electromagnetic component in a hadronic shower will affect the energy resolution in proportion to the ratio $\langle E_{\text{visible, e.m.}}\rangle / \langle E_{\text{visible, hadron}}\rangle$ = "e/h"; hence this value provides a good estimate of the performance of a calorimeter material.

Our group at CERN [2] has proposed to compensate for BE losses and hence to improve the energy resolution by exploiting the additional energy produced in the fission of U-238. This isotope has a very high fission cross-section for n's in the MeV-range, which is precisely the energy range of the evaporated neutrons. Table 5 summarizes the relevant fission cross-sections; the additional measurable energy due to fission appears mostly in form of low-energy (∿ MeV) γ's, which Compton-scatter in the U and L Ar (mean free path of a 1 MeV $\gamma \approx 5$ gaps).

The effect of this compensation can best be judged from Fig. 4. Whereas the e/h value for Fe/L Ar is ∿ 1.35 ± 0.03, it decreases to 1.00 ± 0.03 for the U-238/L Ar. Fig. 5 summarizes the resolution measured for both the Fe/L Ar and the U-238/L Ar calorimeter. The latter measures 10 GeV/c $\pi^{\pm}$'s with a resolution $\sigma = 7.6\%$.

REFERENCES

1) E.B. Hughes et al., Nuclear Instrum. Methods 75, 130 (1969).

2) C.W. Fabjan, C. Kourkoumelis, A. Lankford, G.C. Moneti, P. Rehak, W. Struczinski and W. Willis, to be published.
P. Rehak, Contribution to this Workshop.

3) L. Baum et al., contribution to this Workshop.

4) J.B. Birks, Proc. Phys. Soc. A64, 874 (1951).

5) T.A. Gabriel et al., Nuclear Instrum. Methods 116, 333 (1974).
T.A. Gabriel, private information.

6) V.S. Murzin, Principles and application of the ionization chamber calorimeter, *in* Progress in Elementary Particle and Cosmic-Ray Physics (eds. J.G. Wilson and S.A. Wouthuysen) (North-Holland Publishing Co., Amsterdam, 1967).

7) W. Busza et al., Phys. Rev. Letters 34, 836 (1975).

8) P.R. Vishwanath et al., Phys. Letters 53B, 479 (1975).

Table 1

Effect	Energy		Comments
	Visible	Invisible	
Side/Back Leakage		X	Correlated with nuclear effects, non-Gaussian
Sampling of energy loss		X	Gaussian, geometry dependent
Saturation in ionization		X	Material dependent
"Noise"	X		Pile-up, non-uniformity, gain-drift calibration errors, etc.
Albedo		X	Non-Gaussian
Excitation energy	X	X	Slow n, p; γ
Binding energy		X	Non-Gaussian
μ, ν prod.		X	
Nuclear amplif.	X		

Table 2

Albedo in % of visible energy

Particle / Material	5 GeV/c π	5 GeV/c p	7 GeV/c p	10 GeV/c π	17.3 GeV/c p
Fe/L Ar				4.0%	
U/L Ar	8%	9%		3.3%	
Fe/L.Sc.			4.3%		1.9%
Reference	(2)	(2)	(5)	(2)	(5)

Table 3

Estimated energy of escaping muons and neutrinos[6]

E_0	40 GeV	300 GeV	1000 GeV
$\frac{E_\nu + E_\mu}{E_0}$	1.3%	0.4%	0.3%

Table 4

Binding energy losses

Particle energy (GeV)	Material	Binding energy in %		Reference
		Visible energy	Incident energy	
$\pi^-/1$	Organic scint.	16%	10%	(5)
$\pi^-/3$	Organic scint.	13%	8%	(5)
$\pi^-/7$	Fe/Scint. A.L. ≈ 40 cm	20%	15%	(5)
$\pi^-/10$	Fe L Ar A.L. ≃ 31 cm	24% ± 4%	17% ± 3%	(2)

Table 5

Energy yield in ^{238}U

Process	Cross-section	Time (nsec)	Energy	Comments
$^{238}U(p,X)$ fragm.	$\sigma_{tot}/\sigma_f \sim 0.8$ $E_0 > 100$ MeV	Prompt	205 MeV per fission	Not of primary interest
$^{238}U(n_{evap},X)$ fragm.	$\sigma \geq 0.5$ b for $1.5 \text{ MeV} < E_n < 15$ MeV	< 50 nsec	∿ 8 MeV as ∿ 1 MeV γ's	$\langle n \rangle_{fission} = 2.63$ Multiplication $M = 1.87$ [∿ 40 n/GeV with $\langle KE \rangle \sim 4$ MeV]
$n(^{238}U, {}^{238}U^*)n'$	$\bar{\sigma} = 2.66$b	< 50 nsec	E_{exc} as ∿ 1 MeV γ's	
$n(^{238}U, {}^{239}U)\gamma$	$\bar{\sigma} = 0.15$b	< 50 nsec	∿ 6 MeV of BE in 1 MeV γ's	

Figure captions

Fig. 1a : Measured radial shower containment in tin.

Fig. 1b : Measured longitudinal shower containment in tin, Fe/L Ar, and U-238/L Ar.

Fig. 2 : Measured sampling fluctuations in the CERN L Ar calorimeter.

Fig. 3 : Average number of evaporated neutrons.

Fig. 4 : Visible energy for hadrons and electrons.

Fig. 5 : Energy resolution of the Fe/L Ar and the U-238/L Ar calorimeter. The dashed line indicates an $E^{-\frac{1}{2}}$ extrapolation normalized to the 10 GeV/c point.

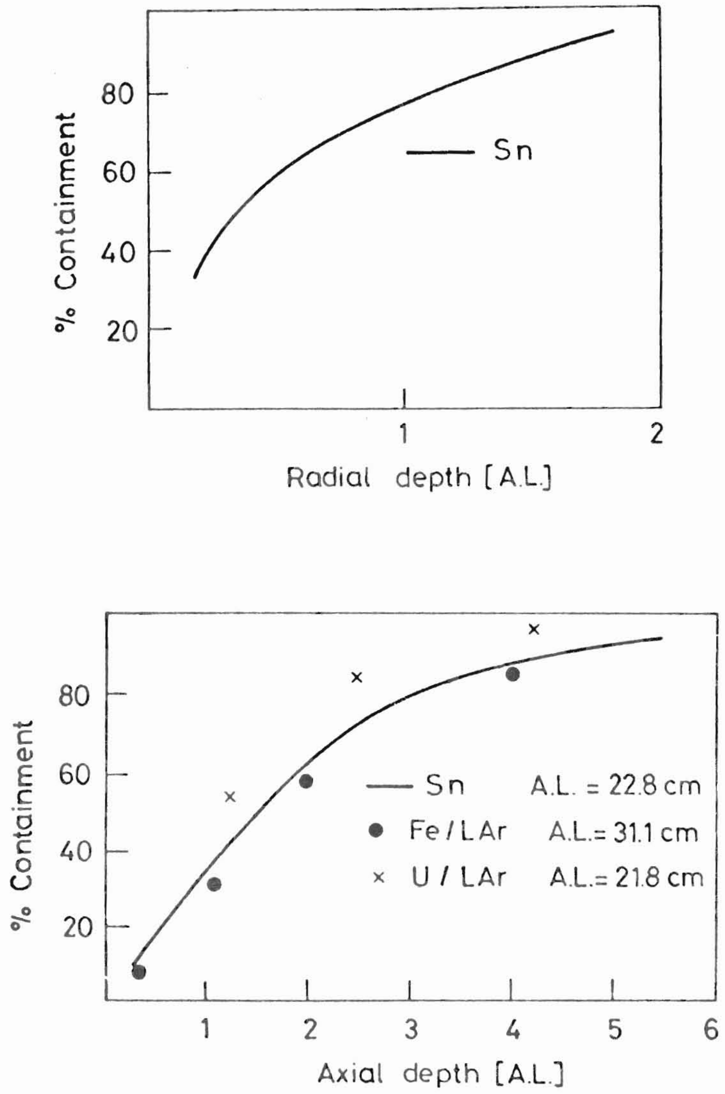
% Containment
80
60
40
20
Sn
1
2
Radial depth [A.L.]
% Containment
80
60
40
20
Sn A.L. = 22.8 cm
● Fe / LAr A.L.= 31.1 cm
× U / LAr A.L.= 21.8 cm
1
2
3
4
5
6
Axial depth [A.L.]

Fig. 1

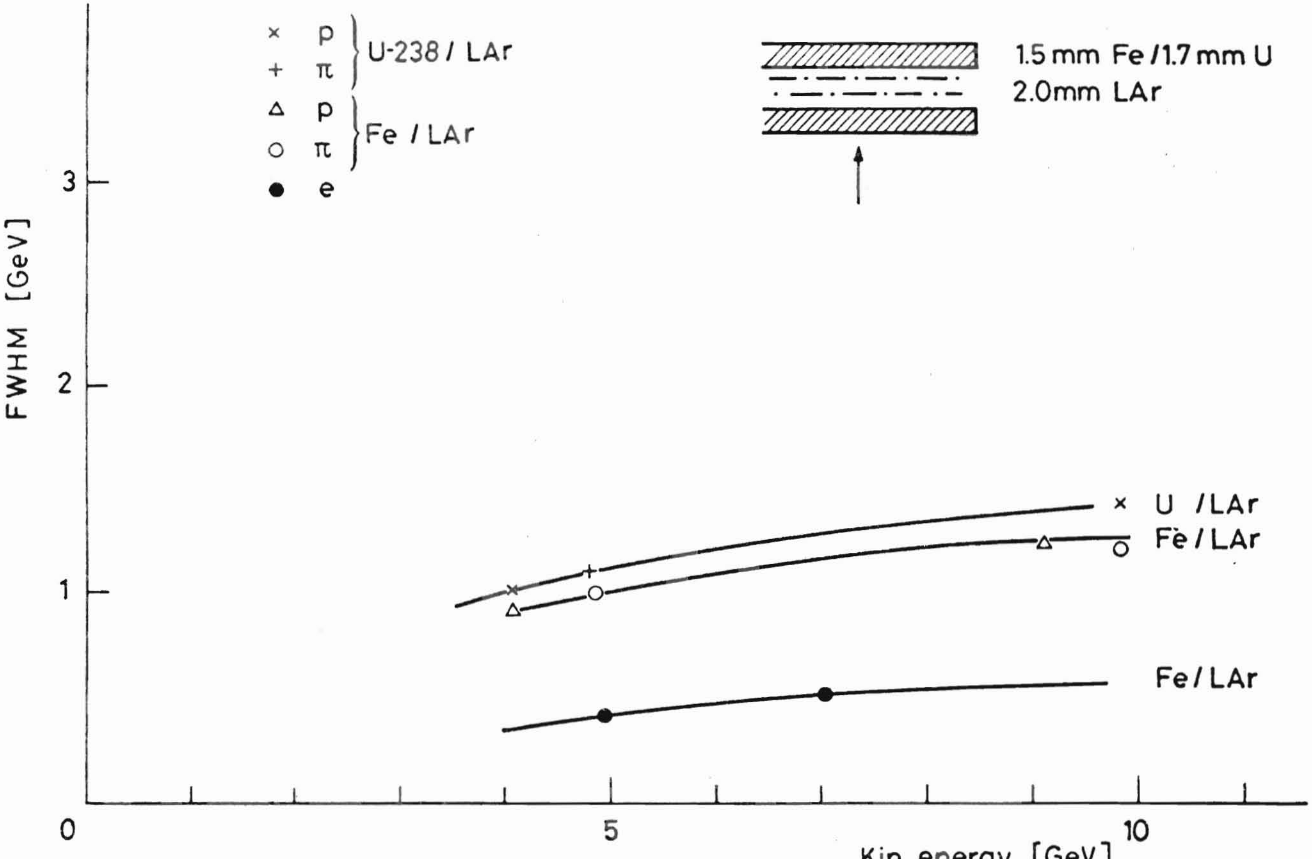
× p
+ π
U-238 / LAr
△ p
○ π
Fe / LAr
● e
1.5 mm Fe / 1.7 mm U
2.0mm LAr
FWHM [GeV]
3
2
1
0
5
10
Kin. energy [GeV]
× U /LAr
Fe / LAr
Fe / LAr

Fig. 2

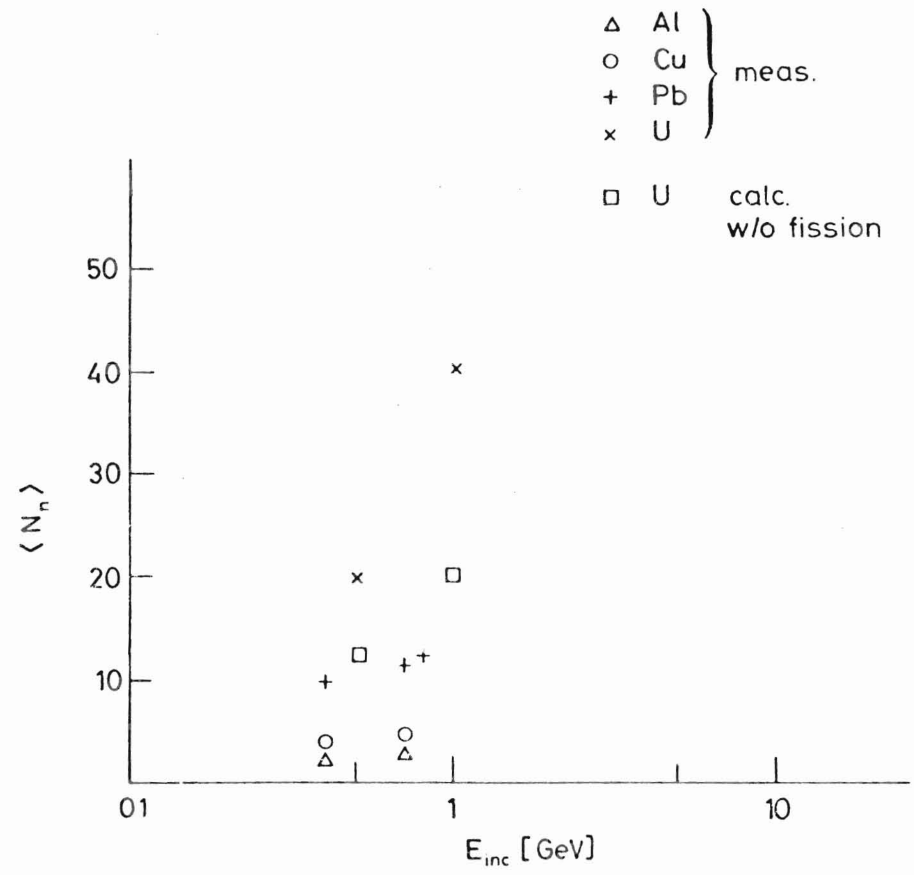

Fig. 3

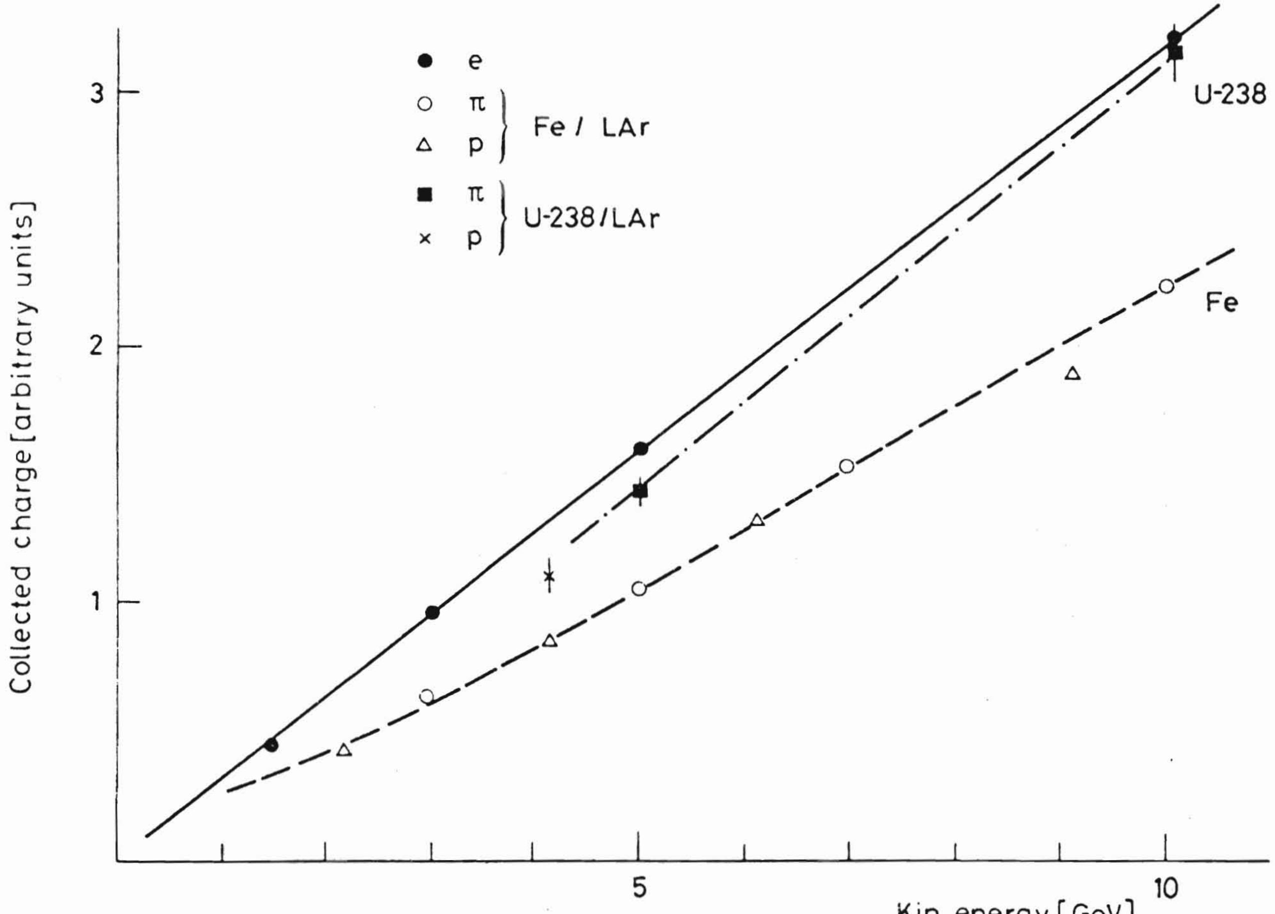
e
π
p
Fe / LAr
π
p
U-238/LAr
U-238
Fe
3
2
1
Collected charge [arbitrary units]
5
10
Kin. energy [GeV]

Fig. 4

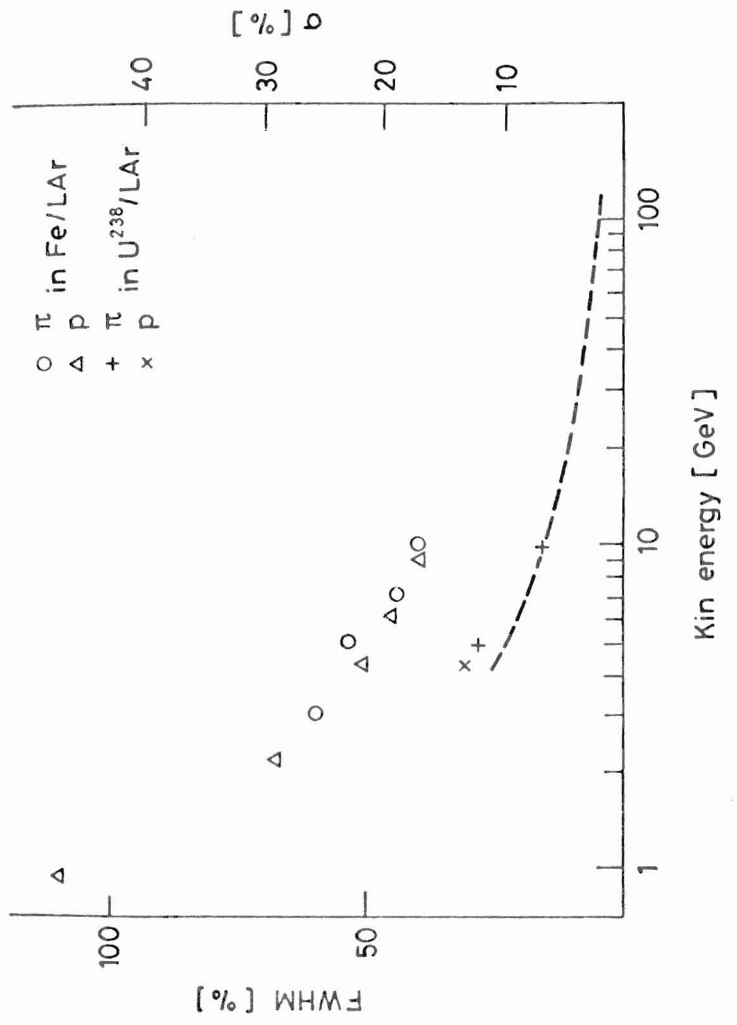
○ π in Fe/LAr
△ p
+ π in U^{238}/LAr
× p
FWHM [%]
100
50
σ [%]
40
30
20
10
1
10
100
Kin energy [GeV]

Fig. 5